just above the two dots relative to that below (*20*). We select here a double-dot sample where $2\delta \sim U - U_{12}$, so we can realize the condition $\mu(1,1) = \mu(0,2)$ at $V = 0$ V.

20. M. Pi *et al.*, *Phys. Rev. Lett.* **67**, 066801 (2001).
21. The precise condition is that $\mu_\ell > \mu(1,1) \geq \mu(0,2) > \mu_r$.
22. D. V. Averin, Yu. V. Nazarov, in *Coulomb Blockade Phenomena in Nanostructures*, H. Grabert, M. H. Devoret, Eds. (Plenum Press and NATO Scientific Affairs Division, New York, 1992), pp. 217–247.
23. Details will be described elsewhere.
24. For $N = 1$, the Coulomb blockade region is initially partially lifted with V because of second-order tunneling when only one state of either dot 1 or 2 is between μ_ℓ and μ_r. In detail, the four thresholds for second-order tunneling marked by faint dotted lines in Fig. 2C are given by the conditions: $\mu(0,1) = \mu_r$, $\mu_\ell = \mu(0,1)$, $\mu_\ell = \mu(0,2)$, and $\mu(1,1) = \mu_r$. These second-order tunneling processes on their own generate a small current. Actually, similar processes are expected inside the $N = 2$ and $N = 3$ Coulomb blockade diamonds bound by solid lines in Fig. 2C, and indeed we see small current features inside these diamonds in Fig. 2B. We do not show the faint dotted lines for the $N > 1$ diamonds in Fig. 2C simply to avoid complexity.
25. Referring to the forward bias potential diagram in Fig. 2A, we consider three possible second-order tunneling processes. Two of them involve elastic tunneling. The first is the case where the electron in dot 1 is virtually scattered to the *2p* state of dot 2 before it exits to the source. The second is the case where the electron in dot 2 virtually exits to the source followed by inter-dot tunneling of the electron in dot 1 to dot 2. The third process involves virtual spin exchange [i.e., the electron in dot 1 (dot 2) is scattered to the nearest contact lead, and an electron of opposite spin is simultaneously scattered back to dot 1 (dot 2) from the same contact lead]. In addition to these second-order tunneling processes, a small current can also be induced by spin flips inside the dot. This, for example, can arise from spin-orbit scattering; however, its contribution is not yet well understood (*26*).
26. T. Fujisawa *et al.*, *Nature*, in press.
27. L. P. Kouwenhoven *et al.*, *Science* **278**, 1788 (1997).
28. One might expect the resonance lines to be parallel to the vertical axis because the resonance condition is, in principle, fulfilled only by adjusting V. However, in practice, they are somewhat tilted because the resonance conditions are slightly modified by changing V_G. Note that these resonance lines terminate on the lowest-lying blue line in Fig. 2B (the threshold for electron tunneling from the drain to the lowest *1s* state of dot 1).
29. At high source-drain voltage beyond the *1s*-*2p* resonance lines, other similar resonance lines are present. The evolution of these resonance lines with B field resembles very closely the familiar Fock-Darwin spectrum for single-particle states in a 2D harmonic potential (*6*, *30*). Hence, we can straightforwardly assign these resonance lines with the *3s*, *3d*,... states in dot 2 (*31*).
30. T. Schmidt, R. J. Haug, K. von Klitzing, A. Förster, H. Lüth, *Phys. Rev. Lett.* **78**, 1544 (1997).
31. K. Ono, D. G. Austing, S. Tarucha, unpublished data.
32. C. Livermore, C. H. Crouch, R. M. Westervelt, K. L. Campman, A. C. Gossard, *Science* **274**, 1332 (1996).
33. We thank T. Fujisawa and M. Stopa for valuable discussions. K. O. and S. T. acknowledge financial support from the Specially Promoted Research, Grant-in-Aid for Scientific Research, from the Ministry of Education, Science, and Culture in Japan and from CREST-JST.

15 February 2002; accepted 16 July 2002
Published online 25 July 2002;
10.1126/science.1070958
Include this information when citing this paper.

Probing Oxygen Motion in Disordered Anionic Conductors with ^{17}O and ^{51}V MAS NMR Spectroscopy

Namjun Kim and Clare P. Grey*

Identification of the local environments of the ions in a solid-state electrolyte that contribute to the ionic conductivity or remain trapped in the lattice represents a challenge for many experimental probes of structure. We show that high-resolution ^{17}O magic angle spinning nuclear magnetic resonance (MAS NMR) spectra may be obtained even from the highly disordered, layered materials α-$Bi_4V_2O_{11}$ and γ-$Bi_4V_{1.7}Ti_{0.3}O_{10.85}$, in which the different oxide sites in the lattice may be distinguished. The sites responsible for anionic conduction were determined directly from the variable-temperature ^{17}O NMR spectra, and correlation times for motion were estimated. Double-resonance ^{17}O/^{51}V NMR methods were used as confirmation of the assignments of the resonances and as a second experimental probe of motion that is sensitive to mobility involving oxide ion hops between the same crystallographic sites.

The ability to draw sufficient power from a fuel cell critically depends on the rate at which ions are transported across the membrane separating the two sources of fuel. For example, the H_2-O_2 solid oxide fuel cell (SOFC) requires rapid oxide ion conduction across an oxide membrane (the electrolyte) (*1*). High oxygen ion conductivity is also essential for a quick response to changes in oxygen partial pressures in a solid-state oxygen sensor and for efficient oxygen separation with oxide membranes (*2*, *3*). The material used commercially in SOFCs and sensors, yttria-stabilized zirconia, does not achieve a conductivity of 10^{-2} S cm^{-1} until 700°C; thus the SOFCs and oxygen sensors are typically operated at temperatures of between 900° and 1000°C and 500°C, respectively (*4*).

The development and optimization of oxide conductors suitable for use at lower temperatures require an understanding of the mechanisms by which anions move in the solid and, thus, a determination of the oxygen sites that contribute to the conductivity and those that remain trapped in the solid. Solid-state nuclear magnetic resonance (NMR) can probe local structure and the local environments of the anions and cations in these inherently disordered materials. Although NMR is also sensitive to dynamics (*5*), it has not been widely applied to study oxide ion motion, in part because the low ionic conduction of most oxides has led to the consequent assumption that motion occurs on a much longer time scale than that probed by magic angle spinning (MAS) NMR. Also, most standard MAS probes can only reach 250°C. High temperatures can be reached with a static probe but at the cost of the spectral resolution. Nonetheless, Adler *et al.* have used wideline and relaxation studies of oxygen mobility to estimate O^{2-} vacancy trapping energies and to investigate O^{2-} mobility at elevated temperatures (*6*, *7*). Here, we extend our previously developed methodology for fluoride systems (*8*, *9*) and report detailed ^{17}O MAS NMR studies of oxide motion in the solid state. We show that a combination of ^{17}O high-resolution MAS and ^{17}O/^{51}V double-resonance [transfer of populations in double resonance (TRAPDOR)] (*10*, *11*) NMR methods may be used to resolve the different crystallographic O sites, to determine which of these sites are responsible for conductivity, and to estimate the rates of exchange between sites.

A series of Aurivillius-type (*12*) oxides $(Bi_2O_2)(A_{m-1}B_mO_{3m+1})$, $Bi_4V_{2-x}Me_xO_{11-\delta}$ (where Me represents a large series of possible dopant cations), have been discovered that show moderate-to-high conductivities near ambient conditions (conductivities of 10^{-4} S cm^{-1} above 200°C for Me = Ti) (*1*, *13*–*16*). These materials can be used as oxygen separation membranes at moderate temperatures (430° to 600°C) (*2*). The idealized version of the structure of $Bi_4V_2O_{11}$ is shown in Fig. 1 and consists of $(Bi_2O_2)^{2+}$ and vanadium oxide perovskite layers. This represents a reasonable model for the high-temperature γ phase. A phase transition to the β phase occurs upon cooling to 570°C, where the vacancies in the perovskite layers partially order to form chains of alternating four- and five-coordinated V atoms (*17*). A further phase transition to the α phase occurs at

---

Department of Chemistry, State University of New York at Stony Brook, Stony Brook, NY 11794–3400, USA.

*To whom correspondence should be addressed. E-mail: cgrey@sbchem.sunysb.edu

450°C, and the V-O-V chains break up to form edge-sharing dimers of five-coordinated V atoms, which are connected to two VO_4 tetrahedra, and isolated, highly disordered $V_2O_7^{4-}$-type units (*17*). The higher-conducting γ phase may be stabilized at room temperature by the appropriate cation [for example, Ti^{4+} (*13*)] substitution. Some of the structural details of the V-O layers are still not completely resolved because the structures, particularly of the α and β phases, are highly disordered and many of the oxygen sites in the V-O layers are only partially occupied. Although it is possible to speculate that the more disordered regions of these solids are associated with higher conductivity, no definitive and direct experimental evidence exists for the relative mobilities of the different sites.

We can distinguish between ions in the perovskite and $(Bi_2O_2)^{2+}$ layers of α-$Bi_4V_2O_{11}$ (*18*) by ^{17}O MAS NMR (Fig. 2). At room temperature, one sharp resonance at 265 parts per million (ppm) and at least two broad isotropic resonances centered at 625 and 830 ppm were observed. The sharp resonance results from at least three similar local environments, because three resonances may be partially separated in a multiple quantum-MAS (*19*) experiment. The resolution is considerably improved at a higher magnetic field strength, and at least seven resonances are observed between 600 and 900 ppm in the spectrum acquired at 14.1 T (Fig. 2B). On the basis of the ^{17}O chemical shift of Bi_2O_3 of 195 ppm (*20*) and the typical chemical shift range for V-O oxygen environments of between 600 and 1000 ppm (*21*), the resonance at 265 ppm was assigned to oxide ions in the $(Bi_2O_2)^{2+}$ layers, and the series of higher frequency resonances was assigned to O^{2-} sites in the vanadate layers. The disorder in the vanadate layers in the α phase accounts for the large number of different ^{17}O resonances.

A previously undetected, sharper ^{17}O NMR resonance was observed at 710 ppm in the low-field spectrum when the sample was heated to 140°C. The resonance was intermediate in chemical shift between the broader resonances at 625 and 830 ppm, indicating that it arose from a chemical exchange process involving oxide ion jumps between the sites that produced the two resonances. The resonance intensified as the temperature was increased, and by 250°C the resonance dominated the spectrum of the V-O region; only a much weaker broad resonance at ~620 ppm remained. Chemical exchange (that is, oxide ion hops) between two different oxide ion sites, with associated resonances separated by a frequency (in Hz) of ν, will first result in line broadening of the two resonances as the jump frequency enters the time scale governed by ν. Coalescence is then observed when the jump frequency = $2^{-1/2}\pi\nu$ (*22*). Thus, the majority of the oxide ions are hopping between sites in the V-O layers with jump frequencies of greater than 22 kHz at 250°C [ν(Hz) = (830 – 625) × 49]. Furthermore, the motion clearly involves oxygen ions in both the "equatorial" (V-O-V) and "axial" (V-O-Bi_n) positions in the perovskite layers.

Again, more detailed chemical information was obtained from the high-field spectra (Fig. 2B). Motion appeared to start on the oxygen sites that produced the resonances at 760 to 650 ppm. Sites that produced higher and lower frequency resonances only became mobile at higher temperatures. The resonances at higher frequency were tentatively assigned to V-O-V linkages with bent V-O-V connectivities (i.e., smaller V-O-V angles) on the basis of the ^{17}O chemical shifts of polyoxometalates (*23*). Linear V-O-V groups resonate at 400 ppm, which suggests that the lower frequency resonances may be assigned to V-O-V with larger bond angles and O atoms coordinated to both V and Bi atoms (the axial V-O atoms) [$BiVO_4$, which contains V-O-Bi_2 local environments, produced two ^{17}O resonances at 500 and 780 ppm (*24*)].

The spinning sidebands of all of the sites, which are due to the ^{17}O satellite transitions, broadened and then disappeared as the tem-

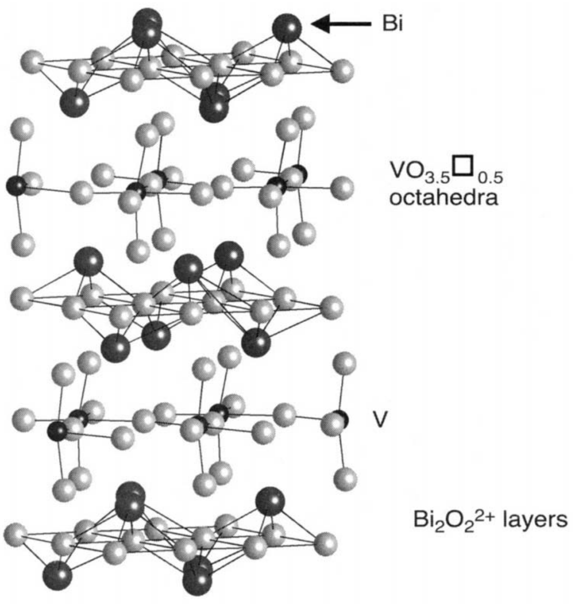

Fig. 1. The idealized structure of $Bi_4V_2O_{11}$. The $VO_{3.5}\square_{0.5}$ groups in the perovskite layers are shown as octahedra, □ indicates a vacancy.

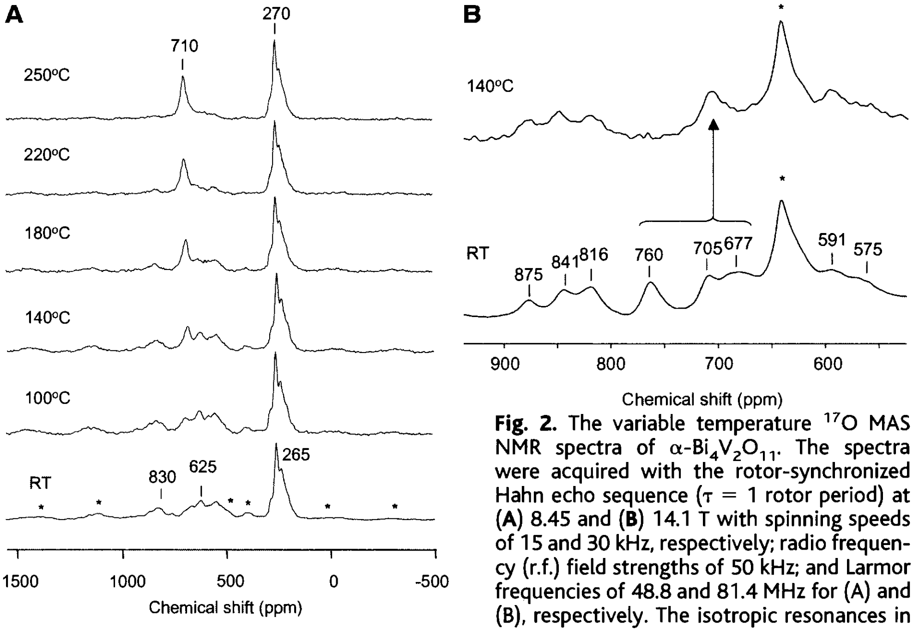

Fig. 2. The variable temperature ^{17}O MAS NMR spectra of α-$Bi_4V_2O_{11}$. The spectra were acquired with the rotor-synchronized Hahn echo sequence (τ = 1 rotor period) at (**A**) 8.45 and (**B**) 14.1 T with spinning speeds of 15 and 30 kHz, respectively; radio frequency (r.f.) field strengths of 50 kHz; and Larmor frequencies of 48.8 and 81.4 MHz for (A) and (B), respectively. The isotropic resonances in (A) are marked by their chemical shift values; the other peaks are spinning sidebands and are marked with asterisks. The asterisks in (B) indicate a spinning sideband that arises from the isotropic resonance at 265 ppm.

perature increased. Motion on a time scale governed by a combination of the MAS and quadrupole coupling constants (QCCs) of the ^{17}O sites will prevent a refocusing of the signals at the rotor echoes, and, hence, the sidebands for systems with large QCCs contain information regarding the process involving slow oxide anion motion. The sharper satellite transitions at room temperature and above (in the 14.1-T spectrum) are due to the $(Bi_2O_2)^{2+}$ oxygen sites and can be simulated to yield a QCC for these sites of 0.8 MHz. The satellite ($|\pm5/2\rangle - |\pm3/2\rangle$ and $|\pm3/2\rangle - |\pm1/2\rangle$) transitions of these sites start to broaden at 140°C in the 14.1-T spectrum and have completely disappeared by 250°C in the 15-kHz MAS, 8.4-T spectrum, which is consistent with motion with a frequency of greater than 10 kHz (*25*). This value is of the same order of magnitude as the value obtained earlier for the jump frequencies of the V-O oxide ions, indicating that the QCCs of the oxide ions in the $(Bi_2O_2)^{2+}$ layers are sensitive to nearby motion that occurs in the V-O layers even though the $(Bi_2O_2)^{2+}$ oxide anions do not directly participate in the hopping process.

Vanadium-51 MAS NMR was used to probe the V coordination environments in these materials (*26–28*). The resonances at –430 (*29*), –440, and –510 ppm, with intensity ratios of 1:4:5.6 (± 0.6), respectively, in the ^{51}V MAS NMR spectra (fig. S1) were assigned to a symmetric tetrahedral; a penta-; and a second, more distorted, tetrahedral V environment, respectively, based on the chemical shift anisotropies previously reported for these resonances (*28*). This intensity ratio is near to the tetrahedral:penta-coordinate V ratio of 2:1 predicted from the crystal structure (*17*). Double-resonance ^{17}O/^{51}V TRAPDOR experiments were then performed in order to investigate V-O connectivity and oxygen mobility (Fig. 3). The double-resonance experiment measures or probes the ^{51}V-^{17}O dipolar coupling, which is directly related to the V-O internuclear distance for a static sample. Only the ^{17}O resonances between 600 and 900 ppm were seen in the ^{17}O/^{51}V difference experiment at room temperature, indicating that these resonances resulted from O sites near V atoms and confirming our earlier assignments. The sharp resonance at 265 ppm was not affected by ^{51}V irradiation, again indicating that it arose from sites in the $(Bi_2O_2)^{2+}$ layers. As the temperature was increased, the spin-spin (T_2) relaxation times of the V-O oxygen atoms decreased noticeably, consistent with the increased motion of these sites. The TRAPDOR effect for the V-O oxygen atoms [which can be quantified with the TRAPDOR fraction, that is, $\Delta S/S_0$, where the ΔS and S_0 are the intensities of a resonance in the difference spectrum and control experiments, respectively (*11*)] decreased considerably at high temperature (150°C; Fig. 3B), indicating the onset of oxide ion motion. The decrease was most pronounced for the resonance at 710 ppm and shows that the ions that contribute to this resonance were hopping between sites on a time scale that was fast in comparison to that governed by the dipolar coupling between the V and O spins (0.5 to 2.5 kHz).

The reverse experiment (^{51}V/^{17}O TRAPDOR NMR) was performed to probe any differences between the mobilities of the ions coordinated to the different V polyhedra. A noticeable effect was seen for all of the sites at room temperature (fig. S2). The TRAPDOR effect dropped dramatically at 250°C for the resonance ascribed to a distorted tetrahedral environment, whereas a sizeable TRAPDOR fraction was still observed for the resonance due to the symmetric VO_4 groups, indicating that the more mobile O^{2-} anions are associated with the more distorted VO_4 groups.

Finally, we used ^{17}O MAS NMR spectroscopy to investigate the more highly conducting titanium-doped γ phase. Motion was considerably enhanced in the vanadium-oxide layers: Even at room temperature, a single resonance at 670 ppm due to mobile oxide ions hopping rapidly between the axial and equatorial positions in the perovskite layers was observed (Fig. 4), with no associated ^{17}O/^{51}V TRAPDOR effect. The resonance sharpened as the temperature was increased to 180°C, indicating higher mobility of the V-O O^{2-} anions. Broadening of this resonance was then observed above 180°C (fig. S3), which is tentatively ascribed to the onset of exchange between the Bi-O and V-O sublattices. The oxide ion motion was not frozen out until –140°C (fig. S3), where a number of broad, overlapping sidebands were resolved due to rigid O^{2-} ions (as demonstrated by the observation of a sizeable ^{51}V/^{17}O TRAPDOR effect at this temperature). Even though the long-range structure of this material is isostructural with that of the more symmetric γ phase, an even larger distribution of O environments is present than in the α phase at low temperatures.

A variety of ^{17}O NMR methods have been used to identify the sublattices that were responsible for anionic conduction. Double-resonance experiments provide a method to detect motion involving jumps between the same crystallographic sites. These jumps will not produce coalescence phenomena, but the motion can be detected by the TRAPDOR experiment. Motion can

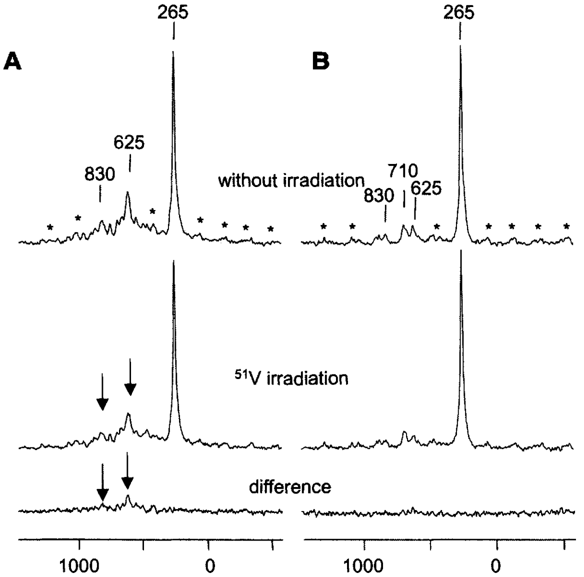

Fig. 3. ^{17}O/^{51}V TRAPDOR experiments at a spinning speed of 10 kHz at (**A**) room temperature and (**B**) 150°C. An r.f. field strength of 100 kHz was used for the ^{51}V irradiation. Spectra were acquired with (double resonance) and without (control) ^{51}V irradiation during the evolution period, τ, of the spin-echo sequence (τ = 4 rotor periods; that is, 400 μs). The difference spectra were obtained by subtracting the two spectra.

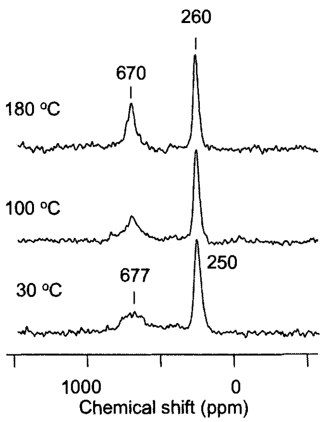

Fig. 4. Variable-temperature ^{17}O MAS NMR spectra of γ-$Bi_4V_{1.7}Ti_{0.3}O_{10.85}$ acquired with a rotor-synchronized Hahn echo sequence (τ = 1 rotor period) and a spinning speed of 18 kHz.

also be detected by broadening the satellite transitions, a third, sensitive method for probing mobility. The rapid conductivity of these materials means that ^{17}O enrichment is simple and efficient. These new approaches, combined with two-dimensional exchange experiments and with the more traditional relaxation methods for probing dynamics, should yield detailed insight into the mechanisms of conduction in a wide range of oxide conductors.

References and Notes

1. J. B. Goodenough, A. Manthiram, P. Paranthanman, Y. S. Zhen, *Solid State Ionics* **81**, 225 (1992).
2. J. C. Boivin *et al.*, *Solid State Ionics* **113–115**, 639 (1998).
3. J.-C. Boivin, *Int. J. Inorg. Mater.* **3**, 1261 (2001).
4. H. L. Tuller, P. K. Moon, *Mater. Sci. Eng.* **B1**, 171 (1988).
5. Z. Xu, J. F. Stebbins, *Science* **270**, 1332 (1995).
6. S. B. Adler, J. A. Reimer, J. Baltisberger, U. Werner, *J. Am. Chem. Soc.* **116**, 675 (1994).
7. S. Adler *et al.*, *Solid State Ionics* **68**, 193 (1994).
8. F. Wang, C. P. Grey, *Chem. Mater.* **9**, 1069 (1997).
9. ———, *J. Am. Chem. Soc.* **120**, 970 (1998).
10. C. P. Grey, W. S. Veeman, A. J. Vega, *J. Chem. Phys.* **98**, 7711 (1993).
11. C. P. Grey, A. J. Vega, *J. Am. Chem. Soc.* **117**, 8232 (1995).
12. B. Aurivillius, *Ark. Kemi.* **1**, 463 (1949).
13. J. Yan, M. Greenblatt, *Solid State Ionics* **81**, 225 (1995).
14. F. Abraham, M. F. Debreuille-Gresse, G. Mairesse, G. Nowogrocki, *Solid State Ionics* **28–30**, 529 (1988).
15. Y. L. Yang, L. Qiu, W. T. A. Harrison, R. Christoffersen, A. J. Jacobson, *J. Mater. Chem.* **7**, 249 (1997).
16. K. R. Kendall, C. Navas, J. K. Thomas, H. C. z. Loye, *Chem. Mater.* **8**, 642 (1996).
17. R. N. Vannier *et al.*, *Solid State Ionics*, in press.
18. α-$Bi_4V_2O_{11}$ and γ-$Bi_4V_{1.7}Ti_{0.3}O_{10.85}$ were prepared from Bi_2O_3 (99.99%), V_2O_5 (99.99%) and TiO_2 (99.9+%) (Aldrich) by heating at 600°C for 12 hours and at 800°C for 24 hours in a platinum crucible. The sample was then enriched in ^{17}O by heating in $^{17}O_2$ gas (Isotec; minimum 50 atom %) at 800°C for 6 hours. The level of enrichment was estimated to be about 30% on the basis of the volume of gas used. X-ray powder diffraction confirmed the purity of both phases.
19. A. Medek, J. S. Harwood, L. Frydman, *J. Am. Chem. Soc.* **117**, 12779 (1995).
20. S. Yang, K. D. Park, E. Oldfield, *J. Am. Chem. Soc.* **111**, 7278 (1989).
21. G. W. Wagner, *Inorg. Chem.* **30**, 1960 (1991).
22. R. K. Harris, *Nuclear Magnetic Resonance Spectroscopy* (Pitman Books, London, 1983).
23. A. T. Harrison, O. W. Howarth, *J. Chem. Soc. Dalton Trans.* 1953 (1985).
24. N. Kim, C. P. Grey, unpublished data.
25. The effective T_2 (T_2^*) for the individual satellite transitions is $\sim 16(\nu_r/\delta)^2\tau_c$, for random isotropic motion, where δ and ν_r are the correction time for motion, the width of the spectrum, and MAS frequencies, respectively [M. M. Maricq, J. S. Waugh, *J. Chem. Phys.* **70**, 3300 (1979)]. The sidebands are no longer resolved when the linewidths of the spinning sidebands are greater than ν_r. An estimate for $T_2^* < 1/\pi\nu_r$ can then be made from $T_2^* < 1/\pi\nu_r$.
26. F. D. Hardcastle, I. E. Wachs, H. Eckert, D. A. Jefferson, *J. Solid State Chem.* **90**, 194 (1991).
27. I. Abrahams *et al.*, *J. Mater. Chem.* **8**, 1213 (1998).
28. F. Delmaire, M. Rigole, E. A. Zhilinskaya, A. Aboukais, G. Mairesse, *Phys. Chem. Chem. Phys.* **2**, 4477 (2000).
29. This resonance is not ascribed to $BiVO_4$ because the ^{17}O resonances expected for this compound are not observed in the ^{17}O spectrum of α-$Bi_4V_2O_{11}$; however, it is difficult to rule out the total absence of this phase.
30. Support from NSF grant DMR-9901308 is acknowledged. M. Ziliox is thanked for help with the 14.1 T NMR experiments; insightful discussions with R. N. Vannier and G. Mairesse are gratefully acknowledged.

Supporting Online Material
www.sciencemag.org/cgi/content/full/1074130/DC1
Figs. S1 to S3

20 May 2002; accepted 9 July 2002

10.1126/science.1074130
Include this information when citing this paper.

Structural Studies of Several Distinct Metastable Forms of Amorphous Ice

C. A. Tulk,[1]*† C. J. Benmore,[2]* J. Urquidi,[2] D. D. Klug,[3]
J. Neuefeind,[2] B. Tomberli,[4] P. A. Egelstaff[4]

Structural changes during annealing of high-density amorphous ice were studied with both neutron and x-ray diffraction. The first diffraction peak was followed from the high- to the low-density amorphous form. Changes were observed to occur through a series of intermediate forms that appear to be metastable at each anneal temperature. Five distinct amorphous forms were studied with neutron scattering, and many more forms may be possible. Radial distribution functions indicate that the structure evolves systematically between 4 and 8 angstroms. The phase transformations in low-temperature liquid water may be much more complex than currently understood.

Amorphous forms of ice have been produced by many techniques. For example, pressurization of ice I to ~13 kbar is known to yield the most common high-density amorphous (HDA) form of ice (*1*). Low-pressure vapor deposition onto a cold target (*2*), rapid quenching of the liquid (*3*), or decompression and heating of the HDA form are known to produce other amorphous forms, all with densities that are similar to that of the crystalline ice I phase. These forms have been categorized as low-density amorphous (LDA) forms. In addition, the LDA form has been reported to abruptly and reversibly transform into the HDA form with the application of pressure, possibly through a first-order phase transition (*4*). This has resulted in the suggestion that all forms of amorphous water can be partitioned into these two high- and low-density forms (*5*). However, a survey of the literature provides the seemingly contradictory view that a continuous range of amorphous structures may exist (*6–10*). In fact, Mishima and others in their original work on the crystalline to amorphous transition stated that "Heating below the 117 K transition causes irreversible changes in the diffraction pattern. . ." (*1*), thus suggesting the possibility of many amorphous forms. However, no detailed structural studies of these possible intermediate forms have ever been reported; therefore, the interpretation of the nature of this important transition is difficult.

Calorimetric studies of this transition have indicated a slow exothermic process followed by a sharp exothermic peak associated with the HDA to LDA transition at 113.4 K at a heating rate of 10 K $hour^{-1}$ (*11*). In addition, subtle differences in the Raman and infrared spectra (*12*, *13*) have been accepted as indicating only minor variations of the more general LDA structural category, and similar claims have been made regarding the HDA category (*7*). Structural studies by neutron and x-ray diffraction (*14–18*) have also resulted in the suggestion that liquid water can be considered a mixture of the low- and high-density forms (*5*). Conversely, relaxation, as indicated by the shift in the first diffraction peak in the HDA form of D_2O upon annealing, has also resulted in the suggestion that some variation in the HDA structure may exist (*7*). Recently, neutron diffraction with isotope substitution experiments on HDA and LDA was also conducted, and the substantial differences in the structures were reported (*19*).

We studied the structural changes during the transition in detail using both neutron and x-ray scattering. We followed the transition continuously by recording the position of the first sharp diffraction peak (FSDP) in the neutron and x-ray static structure factor as a function of time at several anneal temperatures. We found that the

---

[1] Oak Ridge National Laboratory, Oak Ridge, TN 37831, USA. [2] Argonne National Laboratory, Argonne, IL 60439, USA. [3] National Research Council of Canada, Ottawa, Ontario K0A 0R6, Canada. [4] Department of Physics, University of Guelph, Guelph, Ontario N1G 2W1, Canada.

*These authors contributed equally to this work.
†To whom correspondence should be addressed. Present address: IPNS Division, Argonne National Laboratory, 9700 South Cass Avenue, Argonne, IL 60439, USA.